UNIVERSITY OF CALIFORNIA SAN DIEGO

Microbial DNA enrichment promotes adrenomedullary inflammation, catecholamine secretion, and hypertension in obese mice

A thesis submitted in partial satisfaction of the

requirements for the degree Master of Science

in

Biology

by

Zhongmou Jin

Committee in Charge:

Professor Wei Ying, Chair
Professor Alisa Huffaker, Co-chair
Professor Matthew Daugherty

2022

The thesis of Zhongmou Jin is approved, and it is acceptable in quality and form for publication on microfilm and electronically.

University of California San Diego

2022

TABLE OF CONTENTS

LIST OF ABBREVIATIONS

LIST OF FIGURES

Acknowledgement

I would like to acknowledge Professor Wei Ying, as the chair of my committee and my thesis advisor, for his fundamental and continuous support. His guidance has been most motivating since the very beginning of this project.

I would like to acknowledge Dr. Hong Gao, who's also a primary researcher in this study, without whose assistance this research would have never been possible. His help is immeasurable in both experiment operation and analytical study.

This work is a reprint of the material as it appears in Microbial DNA enrichment promotes adrenomedullary inflammation, catecholamine secretion, and hypertension in obese mice. Gao, H., Jin, Z., Tang, K., Ji, Y., Suarez, J., Suarez, J. A., Cunha e Rocha, K., Zhang, D., Dillmann, W. H., Mahata, S. K., & Ying, W. (2022). Journal of the American Heart Association, 11(4). The thesis author is an author of this paper.

ABSTRACT OF THE THESIS

Microbial DNA enrichment promotes adrenomedullary inflammation, catecholamine secretion, and hypertension in obese mice

By

Zhongmou Jin

Master of Sciences in Biology

University of California San Diego, 2022

Professor Wei Ying, Chair
Professor Alisa Huffaker, Co-Chair

Obesity is an established risk factor for hypertension. Building upon the known fact that obesity-induced gut barrier breach leads to the leakage of various microbiota-derived products into host circulation and distal organs, this study seeks to explore impacts of

microbial DNA enrichment on inducing obesity-related adrenomedullary abnormalities and hypertension. CRIg (Complement receptor of the immunoglobulin superfamily) abundance is identified as a major factor in blocking the infiltration of gut mEVs (microbial DNA-containing extracellular vesicles) into the bloodstream and adrenal glands. In lean CRIg-/- or C3-/- mice intravenously injected with gut mEVs, adrenal microbial DNA accumulation elevated adrenal inflammation and norepinephrine secretion, concomitant with hypertension. In addition, microbial DNAs promoted inflammatory responses and norepinephrine production in PC12 cells treated with gut mEVs. Depletion of microbial DNA cargos markedly blunted the effects of gut mEVs. We also validated that activation of cGAS/STING signaling is required for the ability of microbial DNAs to trigger adrenomedullary dysfunctions in both in vivo and in vitro experiments. Restoring CRIg+ cells in obese mice decreased microbial DNA abundance, inflammation, and hypertension. The leakage of gut mEVs leads to adrenal enrichment of microbial DNAs that are pathogenic to induce obesity-associated adrenomedullary abnormalities and hypertension. Recovering CRIg+ macrophage population attenuate obesity-induced adrenomedullary disorders.

Introduction

Obesity is recognized as an independent risk factor for arterial hypertension. It has been reported by the Framingham Heart Study that 60-70% of essential hypertension results from obesity, and obese patients are 3.5 times more susceptible to develop high blood pressure[1, 2]. Although various mechanisms underlying obesity-associated hypertension have been suggested, including increased sympathetic tone[3-5], overactivation of the renin-angiotensin system[6], elevation of aldosterone levels, endothelial dysfunction[7], and mechanical compression of the kidney[8], it is yet to be established how obesity triggers the above changes to cause hypertension. Since dysregulated secretion of norepinephrine (NE) and epinephrine (EPI) is a feature in chronic obesity in both animal models and humans[9], we seek to explore whether microbial DNA enrichment owing to obesity-induced increase in gut permeability causes inflammation of the adrenal medulla[10], resulting in increased secretion of catecholamines and the subsequent development of hypertension. While chronic and low-degree tissue inflammation is a hallmark of obesity, the role of obesity-induced adrenal inflammation in mediating the adrenomedullary function is much less clearly defined[10-12].

Gut barrier breach is one of the characteristics of obesity, resulting in elevated levels of translocation of microbiota-derived products into host circulation and distal tissues[13-18]. Compelling evidence indicates that obesity is concomitant with microbial DNA enrichment in host circulation and tissues[19-23]. In addition, several studies have suggested that circulating microbial DNA species could be biomarkers which precisely mirror the stages of metabolic disease development[19, 22, 24]. Extracellular vesicles (EVs) are important carriers harboring various cargos, such as RNAs, DNAs, lipids, and proteins, and transporting in circulation and

between the neighbor or distant cells[25]. It has been known that microbiota can secrete EVs[26, 27]. More importantly, our previous study has shown that microbiota-derived bacterial DNA-containing EVs (mEVs) are readily translocated from gut lumen into host bloodstream and distal metabolic tissues in obesity, resulting in obesity-related tissue inflammation and insulin resistance[28]. Therefore, these lead us to hypothesize that, in the context of obesity, gut mEVs could infiltrate into adrenal glands and cause microbial DNA accumulation that triggers adrenomedullary inflammation and dysfunction.

While liver immunoglobulin superfamily (CRIg)+ macrophages play important roles in filtering bacteria and their byproducts in the bloods flowing from the intestine through the hepatic portal vein, there is a remarkable reduction in CRIg+ macrophages in the context of obesity[28-30]. We have shown that CRIg+ macrophages can capture gut mEVs from the bloodstream through a complement protein C3-mediated mechanism, whereas depletion of either CRIg or C3 leads to the spread of gut mEVs into distal tissues[28, 30-33]. In addition to liver, CRIg+ macrophages also reside in other tissues such as pancreatic islets[34, 35]. An early study also reports that human adrenal glands harbor a high level of CRIg+ macrophages[30]. However, whether adrenal gland resident CRIg+ macrophages exert protection from the infiltration of gut mEVs and bacterial DNA accumulation is still unknown.

Here, we report that microbial DNA enrichment causes adrenomedullary dysfunction in the context of obesity, resulting in elevated circulating NE levels and the subsequent development of hypertension. Adrenal gland CRIg+ macrophages exert sufficient protection from the penetration of gut mEVs, whereas these CRIg+ cell population is greatly reduced in

obese adrenal glands. We further confirm that microbial DNA cargos contribute to the effects of gut mEVs by activating the cGAS/STING pathway in adrenal chromaffin cells.

Methods

Animal care and use

cGAS$^{-/-}$ (Stock No. 026554), C3$^{-/-}$ (Stock No. 029661), ROSA26iDTR (Stock No. 007900) and Clec4f-Cre (Stock No. 033296) mice were received from the Jackson Laboratory. CRIg$^{-/-}$ mice (C57BL/6J background) were a generous gift from Dr. Wenxian Fu (University of California, San Diego). CRIg wild type (WT) mice were produced by crossing CRIg heterozygous mice together. All mice were maintained on a 12/12 hr light-dark cycle. At 8 weeks of age, male mice were used as recipients for EV injection or fed ad libitum on a high-fat diet (HFD; 60% fat calories, 20% protein calories, and 20% carbohydrate calories; Research Diets) or a normal chow diet (NCD, Lab Diet) for various durations. Germ-free (GF) C57BL/6 mice were maintained in the UCSD Gnotobiotic Mouse Facility. GF mice were fed an irradiated sterilized 60% HFD (06414 Teklad). To deplete Kupffer cells (KC), diphtheria toxin (DT) was intraperitoneally (200 ng/mouse, i.p.) injected into Clec4fCre^{+}DTR^{+} lean mice (KC-KO) for three days, and these mice were treated with DT (200 ng/mouse) every two days to prevent KC recovery. For tissue collection, mice were anaesthetized with an i.p. injection of ketamine (100 mg/kg) and xylazine (10 mg/kg) followed by euthanization by cervical dislocation. All animal procedures were done in accordance with University of California, San Diego Research Guidelines for the Care and Use of Laboratory Animals and all animals were randomly assigned to cohorts when used.

Mouse blood pressure (BP) detection

Non-invasive tail-cuff measurement of BP. The systolic blood pressure (SBP) was also measured indirectly using tail cuff plethysmography in mouse tail-cuff blood pressure system (MRBP; IITC Life Sciences Inc. Woodland Hills, CA) as described previously[36]. Prior to any measurements, the plexiglass restrainers were warmed in 34°C warming chambers for 20 minutes. The mice were then loaded into their restrainers and allowed to incubate in the same warming chambers for 10-15 min. The tails were placed inside inflatable cuffs with a photoelectric sensor that measured tail pulses. The SBP was measured over 5 separate days with an average of at least two well-defined BP cones detected by the tail cuff plethysmograph per day.

Measurement of catecholamines

Mice were anesthetized by inhalation of isoflurane and blood was collected from the heart in potassium-EDTA tubes. Plasma catecholamines were measured by ACQUITY UPLC H-Class System fitted with an Atlantis dC18 column (100A, 3 µm, 3 mm x 100 mm) and connected to an electrochemical detector (ECD model 2465) (Waters Corp, Milford, MA). The mobile phase (isocratic: 0.3 ml/min) consisted of phosphate-citrate buffer and acetonitrile at 95:5 (vol/vol). The data were analyzed using Empower 3 software (Waters Corp, Milford, MA). Catecholamine levels were normalized with the recovery of the internal standard 3,4-Dihydroxybenzylamine (DHBA). Catecholamines were expressed as nM (plasma) or ng/mg protein (PC12 cells) or pg/mg protein (kidney).

***In vivo* and *in vitro* EV treatment.**

For *in vitro* assays, $1x10^7$ EVs as determined by NanoSight analysis were added to $0.1x10^6$ for 24 hours. In addition, for *in vitro* PC12 catecholamine production assay, $5x10^8$ EVs were added to $5x10^6$ PC12 cells. For *in vivo* treatment, recipient mice were tail vein injected with $5x10^9$ EVs twice per week. Our previous study has shown that the amount of bacterial DNAs within $5x10^9$ gut mEVs isolated from HFD WT mice is closed to the abundance of bacterial DNAs in the bloodstream of 16wks HFD WT mice[28].

EV purification and characterization.

The intestinal EVs were prepared from small intestine lumen contents of 16wks HFD mice with sterile tools. Debris and dead cells in the lumen contents were removed by centrifugation at 1,000 x g for 10 min and then filtered through a 0.2 μm filter. The supernatant was then subjected to ultracentrifugation at 100,000 x g for 4 hours at 4°C with a Type 70 Ti fixed-angle rotor (Beckman Coulter). The EV-containing pellet was resuspended in 1 ml sterile PBS and passed through a 0.2 μm filter to remove large particles. The particle size and concentration of intestinal EVs were measured by NanoSight analysis (Malvern Instruments, Westborough, MA). For electron microscopy, EVs were fixed with 2% paraformaldehyde and loaded on Formvar and carbon-coated copper grids. Then the grids were placed on 2% gelatin at 37°C for 20 min, rinsed with 0.15 M glycine/PBS and the sections blocked using 1% cold water fish-skin gelatin. Grids were viewed using a JEOL 1200EX II (JEOL) transmission electron microscope and photographed using a Gatan digital camera (Gatan). To monitor EV trafficking, EVs were labeled with PKH26 fluorescent dye

using the PKH26 fluorescent cell linker kit (Cat. No. PKH26GL-1KT, Sigma). After PKH26 staining, the EVs were washed with sterile PBS and collected by ultracentrifugation (100,000 x g for 2 hours) at 4^{o}C. Finally, PKH26 labeled EVs were resuspended in sterile PBS and the particle concentration was calculated by NanoSight analysis.

***In vivo* EV trafficking assays.**

PKH26-labeled EVs ($5x10^{9}$ EVs per mouse) were delivered to either NCD or HFD recipient mice through either injection into tail vein or jejunum section. After 16 hours EV injection, adrenal glands were collected for detecting the appearance of PKH26 red fluorescence.

DNA depletion in intestinal EVs.

The intestinal EV pellet was dissolved in 100 µl PBS. As previously described, these EVs were loaded into a Gene Pulser/micropulser Cuvettes (Bio-Rad) for electroporation (GenePulser Xcell electroporator, Bio-Rad) and then treated with DNase I (300U) for 30 mins, 37^{o}C. The depletion of bacterial DNAs was confirmed by 16s rRNA qPCR analysis.

Quantification of bacterial DNA using real-time PCR.

Levels of bacterial DNAs were assessed by qPCR using a Femto Bacterial DNA Quantification Kit (Cat. No. E2006, Zymo Research) by following the manufacturer's instructions. Briefly, bacterial DNAs were extracted from EVs or plasma using the ZymoBIOMICS DNA extraction kits (Cat. No. D4301, Zymo Research) according to the manufacturer's instructions. The concentration of bacterial DNA in each sample was determined from the standard curve using a nonlinear regression four-parameter variable slope analysis.

siRNA transfection.

siRNA-cGAS (Cat. No. J-055608-09-0002, Horizon; 20 pmol siRNA/0.1 x 10^6 PC12 cells) was transfected into recipient cells with the lipofectamine RNAiMAX reagent (Cat. No. 13778075, ThermoFisher). siRNA-cGAS was mixed with RNAiMAX reagent and then incubated at room temperature for 15 mins. This mixture was added into the medium of cells. After 24 hours, cells were collected and measured.

CRISPR-Cas9 system for transcriptional activation.

Plasmids containing deactivated Cas9-VPR (VP64, p65, and Rta) system (Cat. No. CAS11915) or guide RNA for Vsig4 (Cat. No. GSGM11893-247477006) were obtained from Horizon. The lentivirus packing these plasmids were prepared by the UCSD Vector core. 12wks HFD WT mice were intravenously injected with these lentiviruses ($1x10^8$ particles/mouse). Control mice were treated with lentivirus containing dCas9-VPR and control gRNA (Cat. No. VSGC10215, Horizon). After 4 weeks, CRIg expression in adrenal glands was evaluated by Western blot analysis.

Immuno-fluorescence staining.

Adrenal glands of NCD or HFD-fed mice were snap frozen in optimum cutting temperature (O.C.T., Fisher Healthcare) with dry ice. Six μm cryo-sections of tissue sections were cut and fixed with pre-cold acetone for 20 min. Slides were blocked with 5% normal donkey serum for 60 min at room temperature. Consequently, the samples were incubated

with anti-CRIg (Cat. No. 17-5752-82, ThermoFisher) antibody diluted 1:100 in PBS at 4 ℃ overnight. After washing, nuclei were stained with DAPI (4',6-Diamidino-2-28 phenylindole dihydrochloride) for 10 min at room temperature. Mounting media and cover slips were then added to slides for imaging. Images were acquired on a Keyence Fluorescent Microscope, and were processed with ImageJ (NIH, Bethesda, MD).

RNAscope in situ hybridization (ISH) combined with immunofluorescence.

We performed RNAscope ISH to detect 16s rRNA. Mouse adrenal glands were frozen in O.C.T with dry ice. Ten µm cryo-sections of tissue sections were prepared and fixed with 4% PFA for 15 min at 4^{o}C and finally dehydrated with 50%, 70%, and 100% ethyl alcohol gradients for 5 min each at room temperature. Tissue sections were then treated by hydrogen peroxide and protease IV at room temperature for 10 min each. 16s RNA probes (Cat. No. 464461, Advanced Cell Diagnostics) were then added for 2 h at 40°C. Signal amplification and detection reagents were applied sequentially and incubated in AMP 1, AMP 2, AMP 3, HRP-C1 (RNAscope® Multiplex fluorescent reagent kit v2, Cat. No. 323100, Advanced Cell Diagnostics), Opal 520 (Cat. No. PNFP1487001KT, Akoya Biosciences), or Opal 690 (Cat. No. FP1497001KT, Akoya Biosciences). Then, samples were immediately processed for immunofluorescence. Images were captured using Leica SP8 Confocal microscope.

Isolation of adrenal chromaffin cells.

Mouse adrenal glands were digested in Hanks' balanced salt solution containing papain (40 U/mL) as described in previous studies [37, 38].

Flow cytometry analysis.

Cells were dispersed and then stained with fluorescence-tagged antibodies. These cells were analyzed by MA900 flow cytometer (SONY). Data were analyzed using Flowjo software.

Quantitative reverse transcriptase-polymerase chain reaction (RT-PCR) analysis.

Total RNA was extracted using the RNA extraction protocol according to the manufacturer's instructions. cDNA was synthesized using SuperScript III and random hexamers (High-capacity cDNA reverse transcription kit, Cat. No. 4368813, ThermoFisher Scientific). qPCR was carried out in 10 μl reactions using iTaq SYBR Green supermix (Cat. No. 172-5125, Bio-Rad) on a StepOnePlus Real-Time PCR Systems (ThermoFisher Scientific). The data presented correspond to the mean of $2^{-\Delta\Delta Ct}$ from at least three independent experiments after being normalized to β-actin.

Western blot analysis.

Cells or tissues were homogenized in RIPA buffer supplemented with protease and phosphatase inhibitors. Equal amounts of cell lysate proteins (30 μg protein per lane for pSTING, 10 μg protein per lane for cGAS or CRIg detection) from each biological replicate were subjected to western blotting. Using ChemiDoc XRS imaging system (BioRad), the protein bands on blots were detected with the SuperSignal West Pico Chemiluminescent Substrate (Cat. No. 34077, ThermoFisher Scientific). Protein bands were analyzed using Image Lab software (BioRad). Western blot data in figures and supplemental figures are all

representative of more than three independent experiments. pSTING (Cat. No. 72971), STING (Cat. No. 50494), and cGAS (Cat. No. 316595) antibodies were obtained from Cell Signaling Technology.

Statistical Analysis.

Tests used for statistical analyses are described in the figure legends. To assess whether the means of two groups are statistically different from each other, unpaired two-tailed Student's *t* test was used for statistical analyses using Prism8 software (GraphPad software v8.0; Prism, La Jolla, CA). *P* values of 0.05 or less were considered to be statistically significant. Degrees of significance were indicated in the figure legends.

Results

Bacterial DNAs are enriched in adrenal glands in the context of obesity.

Previous studies have shown that obesity is accompanied with the accumulation of bacterial DNAs in host circulation and tissues[22, 24, 28]. In line with these findings, we detected high levels of 16s rRNAs in the adrenal glands of 16 weeks high fat diet (16wks HFD) fed WT mice, whereas no bacterial DNA was detected in lean adrenal glands (Figure 1A). In addition, qPCR analysis with 16s rRNA primers indicates that obese adrenal glands harbored much more 16s rRNAs, compared to barely detectable 16s rRNA abundance in lean adrenal glands (Figure 1B). Concomitant with bacterial DNA enrichment in obesity, there were greater levels of proinflammatory cytokines in the adrenal glands of obese WT mice than that in lean WT mice (Figure 1C). To examine the impact of external bacterial DNA contamination during these experiments, we also measured 16s rRNA abundance in the

tissues of HFD-fed germ-free mice using the same protocol. As shown in Figure S1A, there was no detectable 16s rRNA in these germ-free tissues, thus validating a minimal level of exogenous bacterial DNA contamination in our assays. In addition, after 2 weeks antibiotics treatment, bacterial DNA abundance was greatly reduced in obese adrenal glands (Figure S1B).

Gut mEVs can pass through the impaired gut barrier into host circulation and distal tissues in the context of obesity[17]. Thus, to assess whether intestinal mEVs are translocated from gut lumen into host adrenal glands, gut mEVs were collected from the small intestinal lumen of 16wks HFD WT mice and labeled with PKH26 red fluorescent dye (Figures S1C-S1F). These PKH26 mEVs ($5x10^9$ EVs/mouse) were injected into the jejunum section of either lean or 12wks HFD/obese WT recipient mice. After 24 hours, we observed robust red fluorescent signals in the adrenal glands of obese recipients, demonstrating the leakage of PKH26 mEVs into adrenal glands in the context of obesity (Figure 1D). By contrast, PKH26 signals were barely detected in the adrenal glands of lean WT recipient mice (Figure 1D). Taken together, these data indicate that obesity-induced impaired gut barrier allows for the translocation of gut mEVs into adrenal glands.

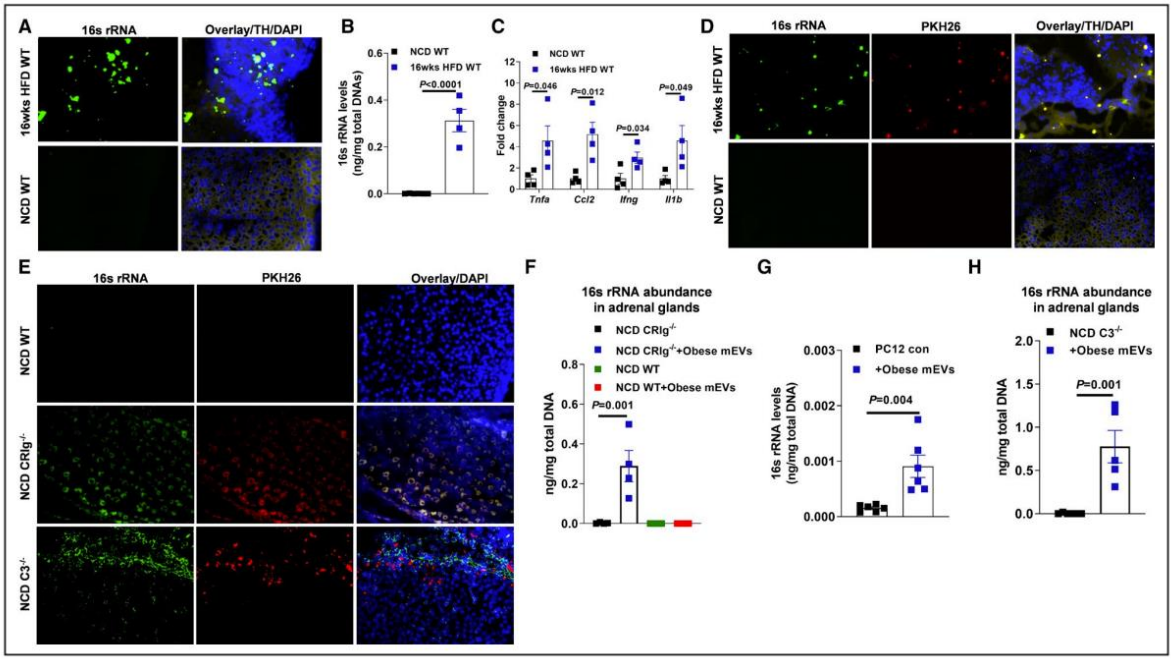

Figure 1. Obesity is associated with bacterial DNA enrichment and inflammation in the adrenal glands. **A**, 16s rRNA abundance in the adrenal glands of both normal chow diet (NCD) or high-fat diet (16 weeks HFD)-fed wild-type (WT) mice. **B**, Quantitative polymerase chain reaction (qPCR) analysis of 16s rRNA abundance in mouse adrenal glands. **C**, The expression levels of proinflammatory genes in the adrenal glands of NCD and 16 weeks HFD WT mice. **D**, The levels of PKH26 red fluorescence and 16s rRNA in the adrenal glands after injection of PKH26-labeled gut microbial DNA-containing extracellular vesicles (mEVs) into the jejunum sections of NCD or 16 weeks HFD WT mice. **E**, The abundance of PKH26 red fluorescence and 16s rRNA in the adrenal glands after intravenous injection of PKH26 gut mEVs into lean WT, CRIg−/− (complement receptor of the immunoglobulin superfamily), or C3−/− (complement component 3) mice. **F**, qPCR analysis of 16s rRNA levels in the adrenal glands of NCD WT or CRIg−/− mice after 4 weeks of treatment with obese mEVs. **G**, The abundance of 16s rRNA in rat pheochromocytoma PC12 cells after 24 hours of treatment with obese mEVs. **H**, 16s rRNA enrichment in the adrenal glands of lean C3−/− mice after 4 weeks of treatment with obese mEVs. Data are representative of 3 experiments (A, D, and E). Data are presented as mean±SEM. P values are determined by unpaired 2-sided Student t test (B, C, G, and H) or 1-way ANOVA analysis (F). DAPI indicates 4’,6-Diamidino-2-28 phenylindole dihydrochloride; TH tyrosine hydroxylase; and 16s rRNA, 16s ribosomal RNA.

Loss of CRIg+ macrophages lead to the infiltration of gut mEVs into adrenal glands.

Our previous study has shown that CRIg+ macrophages play a critical role in blocking the translocation of gut mEVs into host tissues, while the population of CRIg+ macrophages is remarkably diminished in both obese humans and mice[28]. Consistently, after an intravenous injection with PKH26 mEVs ($5x10^9$ EVs/mouse), we observed that red fluorescent signals were spread in the adrenal glands of lean $CRIg^{-/-}$ mice (Figure 1E). Given that gut EVs harbored bacterial DNAs, the spread of gut EVs led to the enrichment of bacterial DNAs in these tissues (Figures 1E and S1E). In addition, qPCR analysis confirmed that 16s rRNA abundance was significantly increased in the adrenal glands of lean $CRIg^{-/-}$ mice after 4wks treatment with gut mEVs ($5x10^9$ EVs/mouse, twice injection per week; Figure 1F). We also observed a remarkable increase in 16s rRNAs within adrenal gland cell PC12 after 24 hours treatment with obese mEVs (Figure 1G).

Complement protein C3 plays important roles in modulating the ability of CRIg+ macrophages to interact with gut mEVs[28, 30]. Consistent with our previous observation, loss of C3 blunted the interaction between CRIg+ macrophages and gut mEVs, as evidenced by robust red fluorescent signals in the adrenal glands of lean $C3^{-/-}$ mice intravenously injected with PKH26 mEVs ($5x10^9$ EVs/mouse; Figure 1E). Concomitant with the infiltration of gut mEVs, bacterial DNAs were enriched in the adrenal glands of lean $C3^{-/-}$ mice injected with gut mEVs (Figure 1H). Thus, these results indicate the importance of CRIg-C3 regulatory axis on blocking the infiltration of gut mEVs.

Gut mEV penetration elevates inflammatory responses and norepinephrine secretion from adrenal medulla.

Given that the infiltration of gut mEVs can results in host cell dysfunction, we next evaluated the impacts of gut mEVs on the responses of adrenal glands in either lean $CRIg^{-/-}$ or $C3^{-/-}$ mice. After 4 weeks intravenous injection with gut mEVs ($5x10^9$ EVs/mouse, twice injection per week), lean $CRIg^{-/-}$ or $C3^{-/-}$ mice displayed elevated levels of inflammatory responses in adrenal glands compared to control mice treated with empty liposomes, as shown by greater abundance of proinflammatory cytokines in adrenal glands (Figures 2A and 2B). In addition, there were greater levels of circulating NE, but not EPI, in lean $CRIg^{-/-}$ or $C3^{-/-}$ mice after 4wks treatment with gut mEVs (Figures 2C and 2D). However, gut mEV treatment did not affect the concentration of NE in kidney and the expression of monoamine oxidase in adrenal glands of lean $CRIg^{-/-}$ mice (Figures S2A and S2B). Consistent with gut mEV-induced increase in circulating norepinephrine levels, we also observed that gut mEVs-treated lean $CRIg^{-/-}$ or $C3^{-/-}$ mice exhibited augmented blood pressure than control mice (Figures 2E and 2F). By contrast, gut mEV treatment had minimal effects on the adrenal gland responses in lean WT mice, as evidenced by comparable levels of adrenal gland inflammation and blood pressure among lean WT recipient mice (Figures 1F, 2G, and S2C). In addition, without gut mEV treatment, lean $CRIg^{-/-}$ mice had comparable blood pressure with lean WT mice (Figure S2D). Given that marked *in vivo* effects of gut mEVs, we also evaluated the direct impacts of gut mEVs on cellular responses in rat pheochromocytoma PC12 cells. After 24 hours of treatment with gut mEVs ($1x10^7$ EVs/$0.1x10^6$ cells), PC12 cells expressed greater levels of proinflammatory cytokines than the control cells treated with empty liposomes (Figure 2H). In addition, gut mEV treatment significantly induced synthesis of NE in PC12 cells (Figures

2I and S2E). We also observed that adrenal chromaffin cells isolated from lean WT mice resulted in increased expression of proinflammatory genes after gut mEV treatment (Figure S2F). Taken together, in the context of loss of CRIg+ macrophages, infiltration of gut mEVs causes functional abnormalities in adrenal glands, contributing to elevated blood pressure.

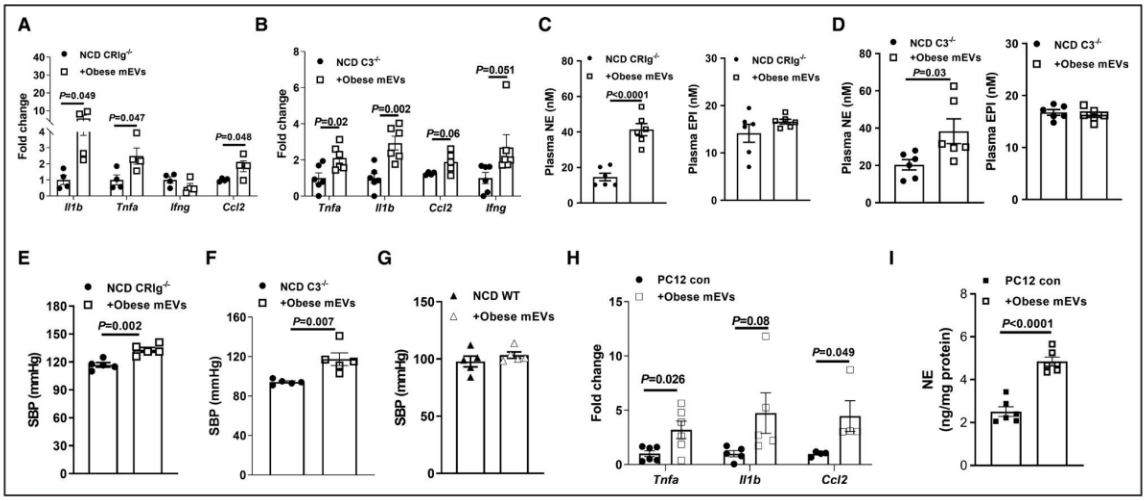

Figure 2. Gut microbial DNA-containing extracellular vesicles (mEVs) induces adrenal inflammation and dysfunction. Quantitative polymerase chain reaction analysis of proinflammatory genes in the adrenal glands of either normal chow diet (NCD) CRIg−/− (complement receptor of the immunoglobulin superfamily) **(A)** or C3−/− (complement component 3) **(B)** mice after 4 weeks of treatment with obese mEVs. The effect of obese mEVs on circulating epinephrine (EPI) and norepinephrine (NE) levels in either lean CRIg−/− **(C)** or C3−/− **(D)** mice. Systolic blood pressure (SBP) levels in either lean CRIg−/− **(E)**, C3−/− **(F)**, or wild-type (WT) **(G)** mice injected with obese mEVs. The abundance of proinflammatory gene abundance **(H)** and NE production levels **(I)** of rat pheochromocytoma PC12 cells after 24 hours treatment with obese mEVs. Data are presented as mean±SEM. P values are determined by unpaired 2-sided Student t test (A through I).

Adrenal gland resident CRIg+ macrophages are sufficient to prevent the effects of gut mEVs.

While liver contains a great amount of CRIg+ macrophages, earlier studies have suggested that adrenal gland is also one of the main sites harboring CRIg+ macrophages[30]. Indeed, we can detect a group of CRIg+ cells in the adrenal glands of lean WT mice (Figure 3A). More importantly, in adrenal glands almost all CRIg signals were co-localized with

F4/80+ cells, suggesting majority of adrenal gland resident macrophages express CRIg (Figure 3A). By contrast, the population of CRIg+F4/80+ cells were greatly reduced in obese adrenal glands (Figures 3A, S3A, and S3B). We next assessed whether adrenal gland CRIg+ macrophages, in the context of knockout of liver CRIg+ macrophages, protect adrenal glands from the infiltration of gut mEVs. Given that in liver CRIg is mainly expressed on Kupffer cells[28-30], Clec4fCre+DTR+ lean mice were treated with diphtheria toxin (200ng/mouse, continuous 3 days intraperitoneal injection) to deplete liver CRIg+ macrophages (KC-KO mice; Figure S3C). In addition, diphtheria toxin treatment did not affect CRIg abundance in adrenal glands (Figures S3D and S3E). More importantly, there was no bacterial DNA detected in the adrenal glands of lean KC-KO mice after 4 weeks intravenous injection with gut mEVs ($5x10^9$ EVs/mouse, twice injection per week; i.p. inject 200ng diphtheria toxin per mouse every 2 days) (Figure 3B). In addition, after 2 hours intravenous injection of PKH26-labeled gut mEVs ($5x10^9$ EVs/mouse), adrenal macrophages in lean WT mice showed elevated PKH26 signals, compared to lean WT control mice without EV injection (Figure 3C). In contrast, in lean $CRIg^{-/-}$ mice, adrenal macrophages failed to capture PKH26 EVs, as evidenced by comparable low levels of PKH26 signals among lean $CRIg^{-/-}$ mice (Figure 3D). Consistent with the absence of bacterial DNAs in adrenal glands after 4wks treatment with gut mEVs, lean KC-KO mice had similar levels of adrenal gland inflammation and blood pressure with control KC-KO mice (Figures 3E and 3F). Thus, these results demonstrate that CRIg+ macrophages residing in adrenal glands exert profound protection from the penetration of gut mEVs.

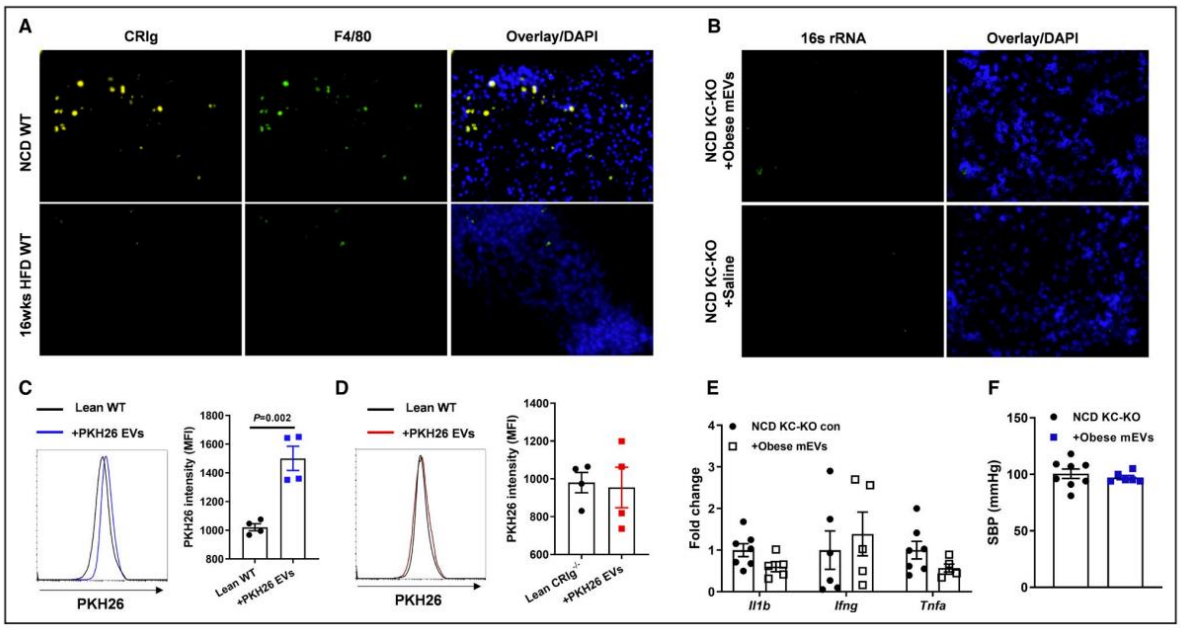

Figure 3. Adrenal gland resident CRIg+ (complement receptor of the immunoglobulin superfamily) macrophages exert profound protection from the infiltration of gut microbial DNA-containing extracellular vesicles (mEVs). **A**, CRIg abundance within the adrenal glands of normal chow diet (NCD) or 16 weeks high-fat diet (16 weeks HFD) wild-type (WT) mice. **B**, The 16s rRNA levels in the adrenal glands of lean Kupffer cell-depleted (KC-KO) mice after 4 weeks of treatment with obese mEVs. After 2 hours of intravenous injection of PKH26-labeled gut mEVs, the intensity of PKH26 signal was detected in adrenal macrophages of lean WT **(C)** or CRIg−/− **(D)** mice by flow cytometry analysis. Lean mice without EV injection were used as controls. After 4 weeks of injection with obese mEVs, proinflammatory gene abundance in the adrenal glands **(E)** and systolic blood pressure (SBP) **(F)** of lean KC-KO mice. Data are the representative of 3 experiments (A and B). Data are presented as mean±SEM. P values are determined by unpaired 2-sided Student t test (C through F). DAPI indicates 4',6-Diamidino-2-28 phenylindole dihydrochloride; EV, extracellular vesicle; KC-KO, depletion of Kupffer cells; MFI, median fluorescence intensity; and 16s rRNA, 16s ribosomal RNA.

Bacterial DNA cargos contribute to the pathogenic effects of gut mEVs.

Concomitant with the infiltration of gut mEVs, the abundance of bacterial DNAs was remarkably elevated in the adrenal glands of lean CRIg$^{-/-}$ or C3$^{-/-}$ mice. In addition, our previous study has demonstrated the critical roles of bacterial DNA cargos within gut EVs[28]. We prepared DNA-free gut EVs using our previously reported method (Figure S4A)[28]. As expected, treatment with DNA-free gut EVs did not cause bacterial DNA accumulation in PC12 cells (Figure S4B). Consistent with our previous findings[28], depletion of bacterial DNA

cargos blunted the effects of gut mEVs, as evidenced by non-significant effects of DNA-free gut EVs on inflammatory responses and NE production in PC12 cells (Figures 4A, 4B, and S4C). In contrast, gut mEV treatment led to functional abnormalities in PC12 cells (Figures 4A, 4B, and S4C). In addition, we confirmed that DNA-free EV treatment did not lead to bacterial DNA enrichment in the adrenal glands of lean CRIg$^{-/-}$ (Figure S4D). More importantly, these CRIg$^{-/-}$ mice had no significant changes in adrenal gland inflammation, circulating catecholamine levels, and blood pressure after treatment with DNA-free gut EVs (Figures 4C-4E). We also confirmed that microbiota-derived EVs contributed to the pathogenic effects of gut EVs, as evidenced by minimal effects of gut EVs collected from 12wks HFD germ-free WT mice on PC12 cells (Figures S1C, S1D, S1F, S4A, and S4E). To test the possibility that bacterial DNA could be bound outside of EV membrane, we treated obese gut mEVs with DNase and then used these EVs to treat PC12 cells. After 24 hours, these gut mEVs resulted in elevated inflammatory responses in PC12 (Figure S4F). Thus, these data demonstrate that microbial DNAs are key cargoes contributing to the pathogenic effects of intestinal EVs.

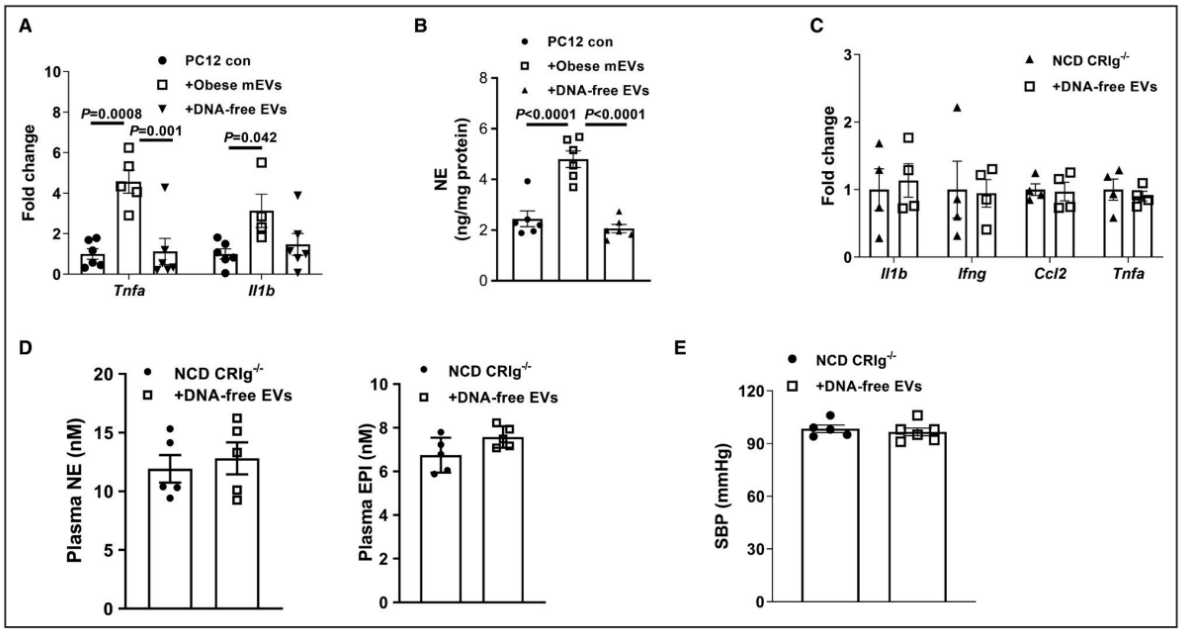

Figure 4. Microbial DNA is pathogenic cargo for the effects of gut extracellular vesicles (EVs). **A**, Quantitative polymerase chain reaction analysis of proinflammatory genes in rat pheochromocytoma PC12 cells after treatment with either obese microbial DNA containing intestinal extracellular vesicles (mEVs) or DNA-free gut EVs. **B**, Effect of obese mEVs or DNA-free EVs on norepinephrine (NE) production of rat pheochromocytoma PC12 cells. Proinflammatory gene abundance **(C)**, circulating catecholamine levels **(D)**, and systolic blood pressure (SPB) **(E)** of normal chow diet (NCD) CRIg−/− (complement receptor of the immunoglobulin superfamily). Data are presented as mean±SEM. P values are determined by 1-way ANOVA analysis (A and B).

cGAS/STING signaling is critical for the ability of microbial DNA to induce adrenal gland dysfunction.

Previous studies, including ours, have demonstrated that the activation of cGAS/STING pathway is required for bacterial DNA-induced cellular responses[28, 39, 40]. Concomitant with bacterial DNA accumulation, we observed an enhancement on the abundance of cGAS and phosphorylated STING in the adrenal glands of obese WT mice, compared to lean WT mice (Figure 5A). After 4wks treatment with gut mEVs, either lean $CRIg^{-/-}$ or $C3^{-/-}$ mice had greater levels of activation of cGAS/STING signaling in adrenal glands (Figure 5B and S5A). In addition, *in vitro* treatment with gut mEVs led to increased

activation of cGAS/STING pathway in PC12 cells (Figure 5C). By contrast, consistent with the absence of bacterial DNA accumulation, gut mEV treatment did not change the abundance of cGAS and phosphorylated STING in the adrenal glands of lean KC-KO mice (Figure S5B).

To further assess the importance of cGAS/STING pathway on the ability of microbial DNAs to induce adrenal gland dysfunction, we compared the adrenal inflammation, circulating catecholamine levels, and blood pressure between 16wks HFD WT and $cGAS^{-/-}$ mice. As shown in Figures 5D-5F, cGAS depletion significantly reduced the levels of obesity-induced adrenal inflammation, plasma norepinephrine levels, and blood pressure, compared to obese WT mice. In addition, another cohort of 8wks HFD $cGAS^{-/-}$ mice were intravenously injected with gut mEVs ($5x10^9$ EVs/mouse, twice injection per week), and control HFD $cGAS^{-/-}$ mice were treated with empty liposomes. After 4 weeks of treatment, there were comparable levels of adrenal gland inflammation and blood pressure among these $cGAS^{-/-}$ mice (Figures 5G, S5C-S5E). In the *in vitro* experiments using PC12 cells pretreated with siRNA-cGAS, we also observed that gut mEVs did not significantly affect cellular responses (Figures 5H, S5F-S5I). Taken together, these results demonstrate the critical role of cGAS/STING signaling for the effects of microbial DNAs on host adrenal cells.

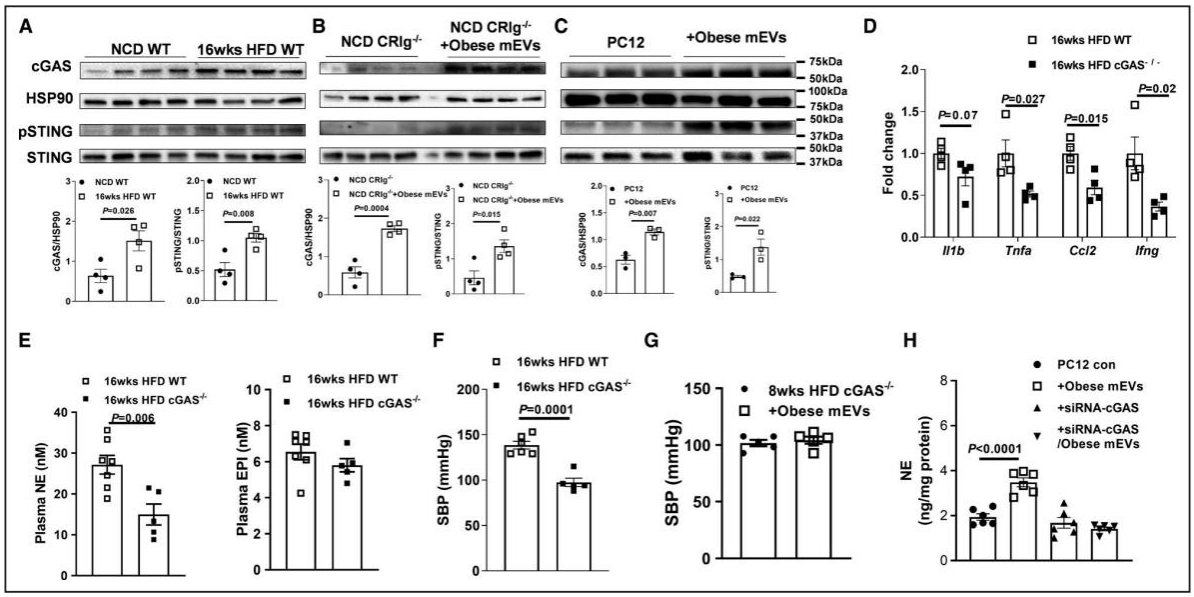

Figure 5. cGAS/STING signaling activation is critical for the effects of microbial DNA. **A**, The abundance of cGAS, phospho-STING, and total STING in the adrenal glands of both normal chow diet (NCD) and 16 weeks high-fat diet (16 weeks HFD) wild-type (WT) mice. B, Effects of obese gut microbial DNA-containing extracellular vesicles (mEVs) on the activation of cGAS/STING signaling in NCD CRIg−/− (complement receptor of the immunoglobulin superfamily) adrenal glands **(B)** or rat pheochromocytoma PC12 cells **(C)**. The levels of adrenal inflammation **(D)**, circulating catecholamine **(E)**, and systolic blood pressure (SBP) **(F)** of 16 weeks HFD WT vs cGAS−/− mice. Effects of obese mEVs on the levels of SBP **(G)** of 16 weeks HFD cGAS−/− mice. H, The norepinephrine (NE) production of rat pheochromocytoma PC12 cells treated with obese mEVs and/or siRNA-cGAS. Data are presented as mean±SEM. P values are determined by unpaired 2-sided Student t test (A through F) or 1-way ANOVA analysis **(H)**. cGAS indicates Cyclic GMP–AMP synthase ; EPI, epinephrine; HSP90, heat shock protein 90; pSTING, phosphorylated STING; siRNA, small interfering RNA; and STING, the cyclic GMP–AMP receptor stimulator of interferon genes.

Restoring CRIg+ macrophage population attenuates obesity-associated adrenomedullary dysfunction.

Given that the critical roles of CRIg+ macrophages in blocking the effects of gut mEVs, we next tested whether recovery of CRIg+ macrophage population could alleviate obesity-induced adrenal disorders. Previous studies have demonstrated that deactivated Cas9 (dCas9) can fuse to the transcriptional activation domains by specifically designed guide RNA (gRNA)[41-44]. In addition, the VPR system (including three transcriptional activators

VP64, p65, and Rta) linked to the C-terminal end of dCas9 activates gene expression (Figure S6A). To reboot the expression of Vsig4 (a gene encoding CRIg), 12 wks HFD WT mice were intravenously injected with lentivirus carrying both deactivated Cas9-VPR system (VP64, p65, and Rta) and gRNA-Vsig4 ($1x10^8$ particles/mouse; HFD CRIgoe). After 4 weeks injection with these lentiviruses, we observed that CRIg+ macrophage population was restored in adrenal glands (Figures S6B). More importantly, compared to 16wks HFD WT control, the levels of bacterial DNAs and inflammatory responses were significantly reduced after recovery of CRIg+ macrophage proportion (Figures 6A-6C), concomitant with decreased levels of circulating norepinephrine and the consequent decrease in blood pressure (Figures 6D and 6E). Thus, these findings indicate that restoring CRIg+ macrophage population mitigates obesity-associated dysregulation of catecholamine secretion and the consequent development of hypertension.

Discussion

It is well-established that obesity is associated with hypertension and is prevalent in both children and adults[2, 45, 46]. Despite intensive research, the mechanisms underlying obesity-induced hypertension are incompletely understood. Existing literature reveals that high calorie loads in patients with obesity increase peripheral NE turnover, which increases sympathetic nervous system (SNS) activity[45, 47]. Diminished baroreflex and insulin sensitivity in obese patients have been implicated in further enhancing SNS activity[48]. Obesity-induced hyperinsulinemia has also been reported to contribute to the development of hypertension through increased sodium retention, causing volume overload as well as endothelial dysfunction and favoring vasoconstriction[45, 49, 50]. Here we provide strong evidence that

enrichment of microbial DNA in the adrenal medulla leads to inflammation of the adrenal medulla resulting in increased catecholamine secretion and the consequent development of hypertension. In fact, we have recently reported that the lack of an anti-inflammatory peptide catestatin results in infiltration of macrophages in the adrenal medulla, causing tissue inflammation, increased catecholamines secretion and hypertension[36]. Inflammation is a key pathophysiologic factor driving hypertension, and obesity is characterized by chronic and low-degree inflammation. Indeed, the world-wide obesity epidemic is paralleling a growth in hypertension prevalence. Therefore, understanding the mechanisms underlying obesity-associated hypertension is necessary for future therapeutic development. In this study we have assessed the impacts of microbial DNA enrichment on the incidence of obesity-associated adrenomedullary inflammation and hypertension. In this study, we find that obesity is associated with high abundance of bacterial DNAs in adrenal glands, concomitant with elevated level of adrenal inflammation. In the context of obesity, gut mEVs are readily translocated into distal adrenal glands and contribute to the enrichment of microbial DNAs in these tissues. By contrast, there were no detectable bacterial DNAs in the adrenal glands of lean/healthy WT mice. We find that adrenal gland resident macrophages are CRIg+ cells and exert profound protection from the infiltration of gut mEVs, whereas the population of these adrenal CRIg+ cells are largely diminished in obesity. In lean $CRIg^{-/-}$ or $C3^{-/-}$ mice treated with gut mEVs, adrenal microbial DNA enrichment results in elevated levels of adrenomedullary inflammation and catecholamine secretion, concomitant with hypertension. In addition, *in vitro* treatment with gut mEVs directly enhances inflammation and catecholamine secretion levels in PC12 cells. By contrast, depletion of microbial DNAs blunts the effects of gut mEVs. However, these results cannot exclude the effects of other pathogenic

factors leaked from gut lumen on obesity-associated adrenal dysfunctions. We also confirm that the activation of cGAS/STING pathway is required for the ability of microbial DNAs to trigger cellular dysfunctions. Finally, rebooting CRIg expression significantly attenuates obesity-associated adrenal disorder.

The leakage of microbiota-derived products is increased in obese humans and animal models, because of the impaired gut barrier[13, 17, 18]. In line with previous findings[22, 24, 28], a great amount of bacterial DNAs was present in the obese adrenal glands. We have demonstrated that microbiota-derived EVs harbored microbial DNAs and played a critical role in delivering these cargos into distal host tissues. There may be other manners resulting the enrichment of bacterial DNAs in host tissues. For example, previous studies suggest that gut microbiota could penetrate through obese gut barrier into host circulation and tissues[19, 20, 51]. However, Zulian et al. reported that there is a rare existence of bacteria in obese host tissues, suggesting that bacteria hardly escape from gut lumen in obesity[52]. Previous studies suggest that healthy gut barrier can selectively allow microbial product secreting into host circulation[53, 54]. However, in our studies gut mEVs cannot pass through healthy intact gut barrier, as evidenced by no detectable red fluorescent signals and bacterial DNAs in the adrenal glands of lean WT mice after injected with PKH26-labeled gut mEVs into jejunum section.

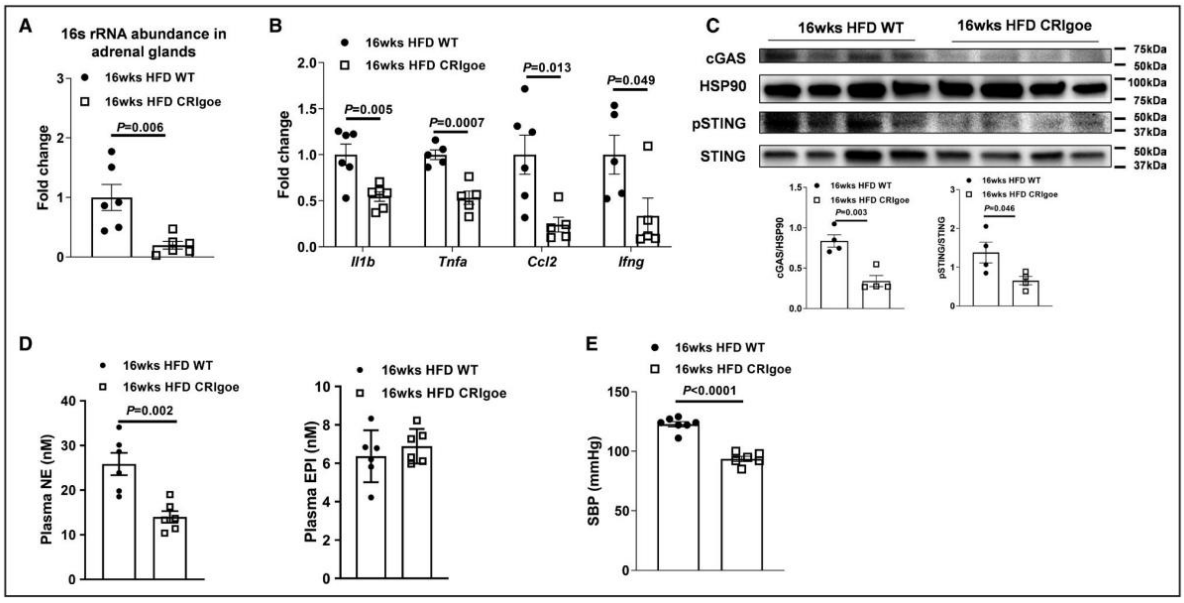

Figure 6. Recovery of CRIg+ (complement receptor of the immunoglobulin superfamily) macrophage population attenuates obesity-associated adrenal dysfunction. After 4 weeks of injection with lentivirus harboring deactivated Cas9 and guide RNA-Vsig4, the abundance of bacterial DNA **(A)**, proinflammatory genes **(B)**, cGAS/STING activation **(C)** in the adrenal glands, circulating catecholamine **(D)**, and systolic blood pressure (SBP) **(E)** of 16 weeks high-fat diet (HFD) wild-type (WT) mice were evaluated. Data are presented as mean±SEM. P values are determined by unpaired 2-sided Student t test (A through E). Cas9 indicates CRISPR associated protein 9; cGAS, Cyclic GMP–AMP synthase; CRIgoe, overexpressing CRIg; EPI, epinephrine; HSP90, heat shock protein 90; NE, norepinephrine; pSTING, phosphorylated STING; STING, the cyclic GMP–AMP receptor stimulator of interferon genes; and Vsig4, V-set and immunoglobulin domain containing 4.

Our previous study has demonstrated the critical role of CRIg+ macrophages in blocking the spread of gut mEVs into host tissues[28]. In addition to liver, consistent with previous findings[30], we also observed that most of adrenal tissue resident macrophages express CRIg in lean WT mice. In contrast, obese adrenal glands contained much less amount of CRIg+ macrophages. Using lean KC-KO mice, we further validated that adrenal CRIg+ macrophages also exerted profound protection from the infiltration of gut mEVs.

It has been well known that obesity is accompanied by chronic and low-degree inflammatory responses in various tissues[11]. Several studies have also reported that both

human and animal adrenal cells can produce proinflammatory cytokines, including IL1β, TNFα, IFNγ, and CCL2, in response to various stress[55, 56]. We also observed that obese adrenal chromaffin cells produced elevated levels of proinflammatory cytokines, suggesting an active inflammatory status in obese adrenal medulla. While previous studies suggest that elevated circulating proinflammatory cytokines can trigger adrenomedullary abnormalities, obesity-induced adrenomedullary production of proinflammatory cytokines may also act as autocrine factors eventuating in adrenal catecholamine secretion disorder[10, 57, 58]. More importantly, in both *in vivo* and *in vitro* experiments we observed that gut mEVs-induced accumulation of bacterial DNAs promoted the production of adrenal proinflammatory mediators, whereas treatment with DNA-free gut EVs had minimal effects on adrenal inflammation. Thus, these findings indicate that bacterial DNAs play important roles in inducing obesity-associated adrenomedullary inflammation and hormonal dysfunction.

Previous studies, including ours, have demonstrated that the cGAS/STING signaling is required for the ability of microbial DNAs to modulate host cell responses[28, 40]. Consistently, there was also improvement in the activation of cGAS/STING signaling in adrenal cells after gut mEV-induced bacterial DNA accumulation in both *in vivo* and *in vitro* assays. More importantly, activation of cGAS/STING signaling plays critical roles in bacterial DNA-mediated adrenomedullary inflammation and catecholamine secretion disorders, as shown by minimal functional changes in cGAS knockout adrenal cells in response to gut mEV treatment. Previous studies also indicate that canonical inflammatory pathways such as NFκB-associated signaling play critical roles in mediating adrenomedullary inflammatory responses[59-61]. In addition to the cGAS/STING pathway, other studies have reported that the toll-like receptor 9 (TLR9) or the absent in melanoma 2 (AIM2) inflammasome exert

profound function on sensing pathogenic DNAs[62, 63]. Endosomal membrane receptor TLR9 specifically detects CpG hypomethylated DNAs to protect from virus and other pathogens[64]. AIM2 inflammasome activation is initiated by double stranded DNAs and leads to proteolytic maturation of the pro-inflammatory cytokines[63]. However, whether TLR9 or AIM2 participate in sensing microbial DNAs in adrenal medulla is still unknown.

Conclusions

In summary, we have shown that microbial DNA accumulation leads to obesity-associated adrenomedullary dysfunctions leading to hypertension. We demonstrate the critical roles of adrenal resident CRIg+ macrophages and put forward a novel concept of how obesity induces hypertension through microbial DNA-induced adrenomedullary abnormalities, thereby providing a potential therapeutic target for obesity-related hypertension.

Acknowledgements

This work is a reprint of the material as it appears in Microbial DNA enrichment promotes adrenomedullary inflammation, catecholamine secretion, and hypertension in obese mice. Gao, H., Jin, Z., Tang, K., Ji, Y., Suarez, J., Suarez, J. A., Cunha e Rocha, K., Zhang, D., Dillmann, W. H., Mahata, S. K., & Ying, W. (2022). Journal of the American Heart Association, 11(4). The thesis author is an author of this paper.

Supplemental Materials

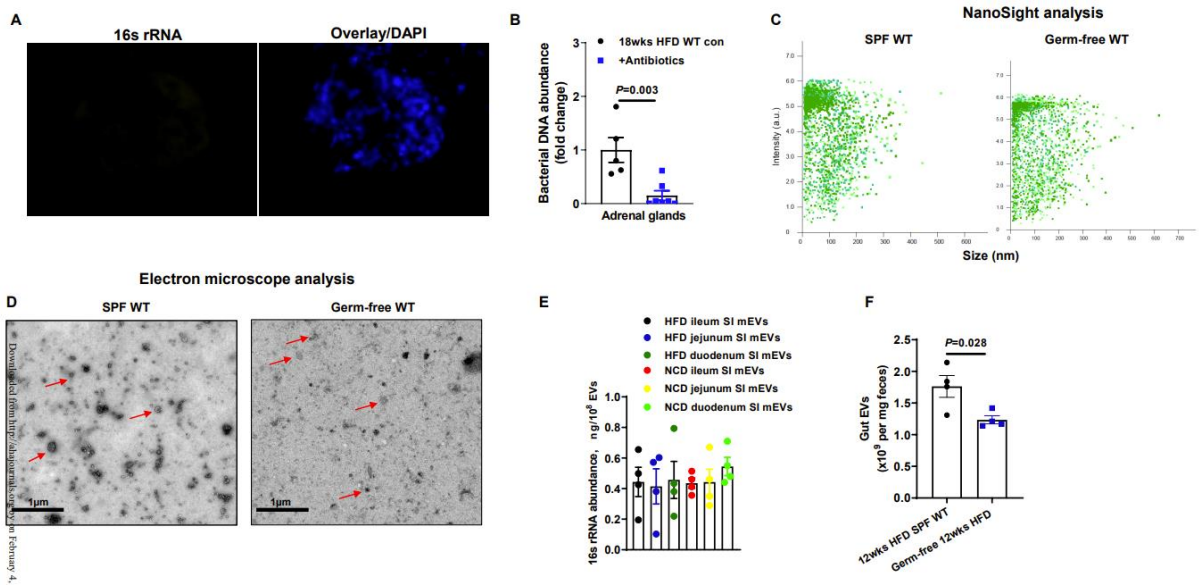

Figure S1. Characteristics of gut mEVs collected from 16wks HFD WT mice, related to Figure 1. **A**, The existence of 16s rRNA in the pancreatic tissue of 16wks HFD germ-free mice. Data are the representative of three experiments. **B**, Bacterial DNA abundance in adrenal glands of obese mice after 2 weeks antibiotics treatment. **C**, The particle sizes of gut EVs were measured by NanoSight analysis. **D**, The morphology of gut EVs examined by electron microscopy analysis. Red arrows indicate extracellular vesicles. **E**, qPCR analysis of 16s rRNA levels in the EVs isolated from small intestinal (SI) lumen of lean WT or 16wks HFD WT mice. **F**, The production of EVs yielded from small intestinal gut lumen contents. NCD, normal chow diet; HFD, high fat diet. SPF, specific-pathogen free. Data are presented as mean ± SEM. P values are determined by unpaired two-side Student's t-test (B and F).

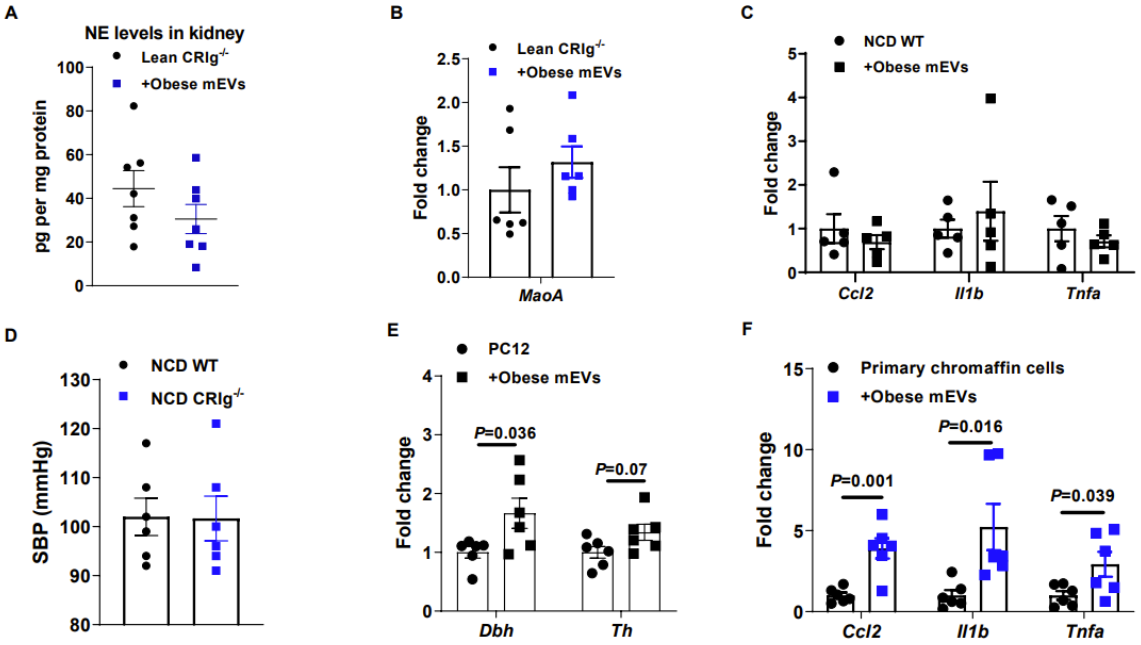

Figure S2. Effects of obese gut mEVs on lean WT mice, related to Figure 2. Norepinephrine (NE) levels in the kidney **(A)** and monoamine oxidase abundance in adrenal glands **(B)** of lean CRIg-/- mice after 4 weeks treatment with gut mEVs. **C**, qPCR analysis of proinflammatory genes in the adrenal glands of lean WT mice after 4wks treatment with obese mEVs. **D**, The levels of systolic blood pressure (SBP) of lean WT and CRIg-/- mice. **E**, The abundance of genes associated with catecholamine synthesis in PC12 cells after 24 hours treatment with obese mEVs. **F**, Effects of gut mEVs on proinflammatory gene expression in primary chromaffin cells isolated from lean WT mice. Data are presented as mean ± SEM. P values are determined by unpaired two-side Student's t-test (E and F).

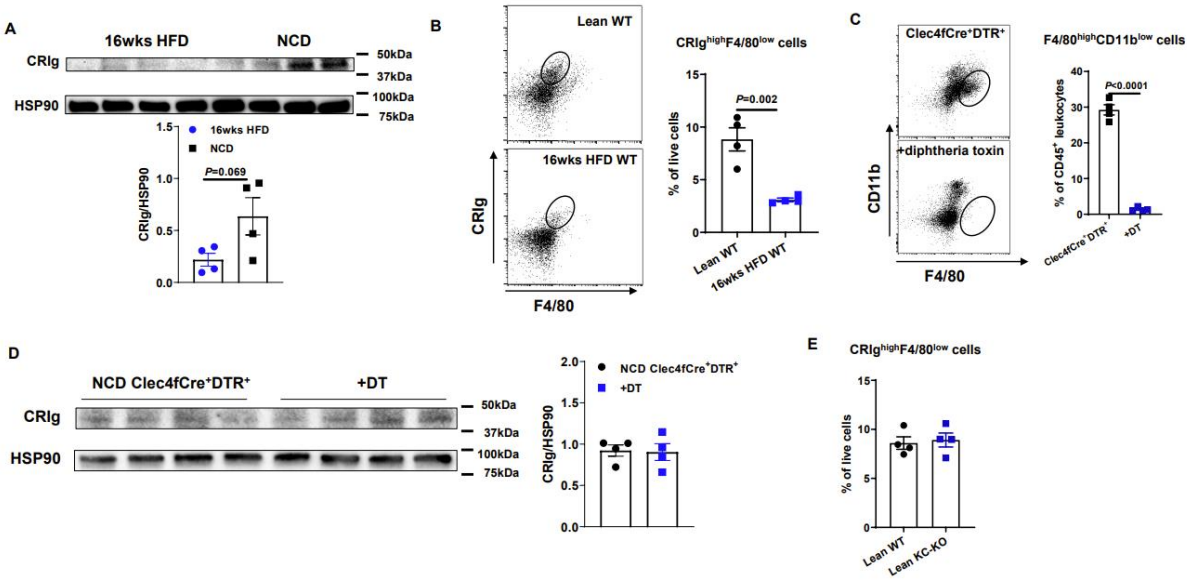

Figure S3. The important roles of adrenal CRIg+ macrophages, related to Figure 3. **A** and **B**, Effect of obesity on CRIg abundance in adrenal glands. **C**, Validation of Kupffer cell (CD11blowF4/80high) depletion after lean Clec4fCre+DTR+ mice injected with diphtheria toxin (DT) (KC-KO). **D**, Effect of DT treatment on CRIg abundance in adrenal glands of lean Clec4fCre+DTR+ mice. **E**, Flow cytometry analysis of CRIg+F4/80+ cells in adrenal glands of lean WT and KC-KO mice. Data are presented as mean ± SEM. P values are determined by unpaired two-side Student's t-test (A-C).

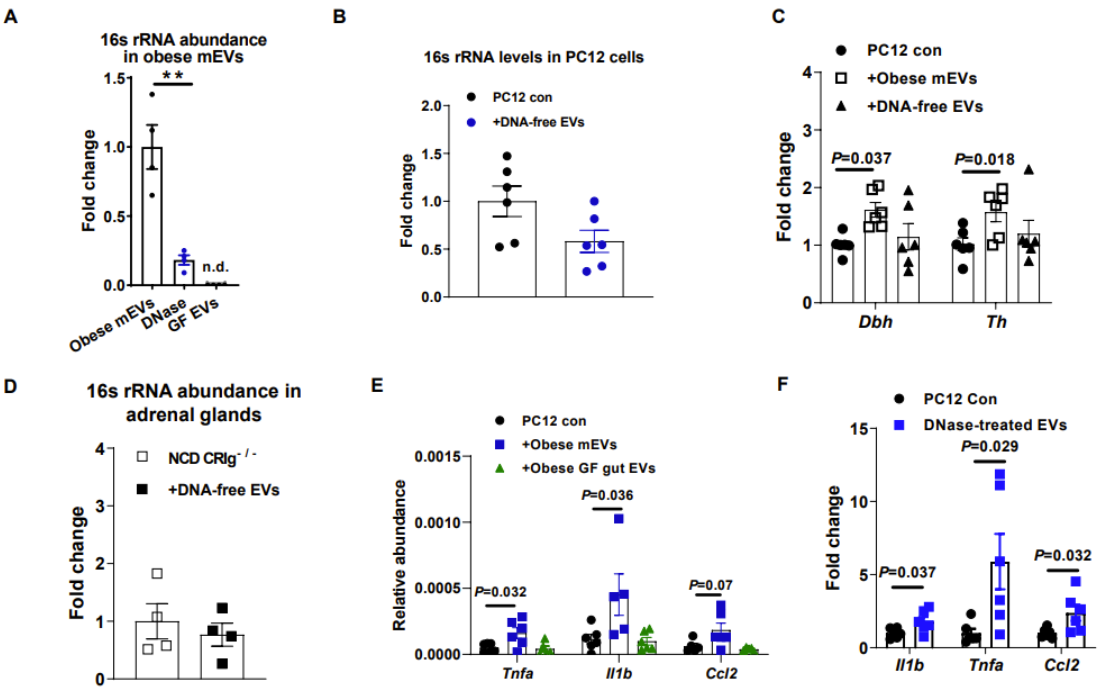

Figure S4. The importance of microbial DNA cargos, related to Figure 4. **A**, qPCR analysis of 16s rRNA abundance within gut EVs after treatment with electroporation and DNase or gut EVs collected from germ-free mice. n.d. non-detectable. 16s rRNA abundance in PC12 cells **(B)** or the adrenal glands of NCD CRIg-/- **(D)** mice after treatment with DNA-free EVs. **C**, The abundance of key genes associated with catecholamine synthesis in PC12 cells after treatment with either obese mEVs or DNA-free EVs. **E**, Effects of germ-free gut EVs (GF gut EVs) on PC12 cell inflammation. **F**, Effects of DNase-treated obese gut mEVs (without electroporation) on PC12 inflammation. Data are presented as mean ± SEM. P values are determined by unpaired two-side Student's t-test (A and F) or one-way ANOVA (C and E).

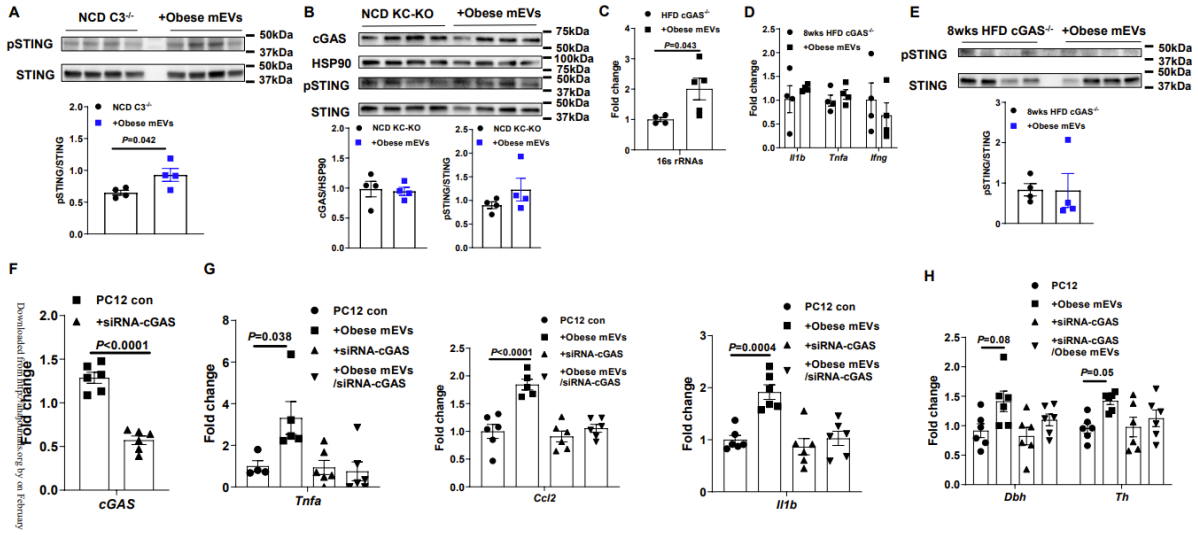

Figure S5. The importance of cGAS/STING activation for the effects of mEVs, related to Figure 5. After 4wks treatment with obese mEVs, the abundance of cGAS/STING in adrenal glands of lean C3-/- **(A)** or KC-KO **(B)** mice. **C**, qPCR analysis of 16s rRNA abundance in adrenal glands after HFD cGAS-/- mice treated with obese mEVs. The abundance of proinflammatory cytokines **(D)** and activation of cGAS/STING **(E)** in adrenal glands of HFD cGAS-/- mice after 4wks treatment with obese mEVs. **F**, Validation of cGAS knockdown in PC12 cells after treatment with siRNAcGAS for 24 hours. The expression of proinflammatory genes **(G)** and genes associated with catecholamine synthesis (H) in PC12 cells after treatment with obese mEVs and/or siRNA-cGAS. Data are presented as mean ± SEM. P values are determined by unpaired two-side Student's t-test (A and F) or one-way ANOVA (G and H).

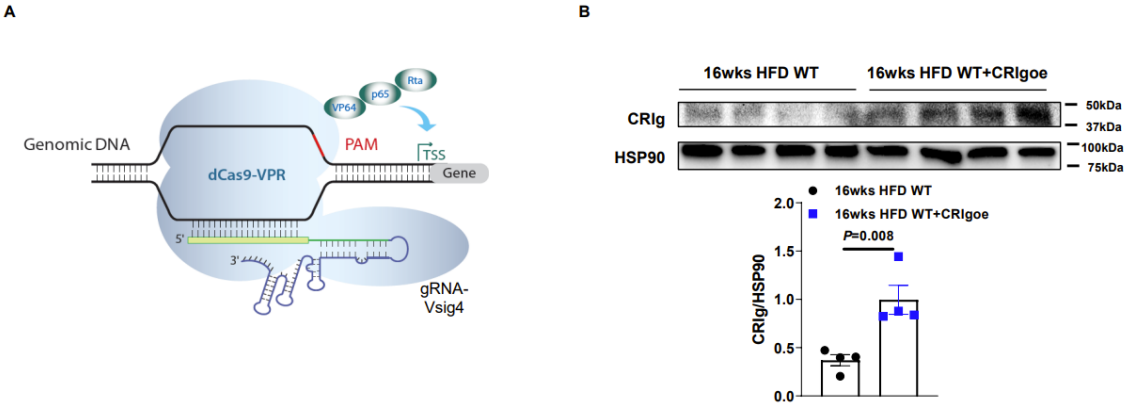

Figure S6. Recovery of Vsig4 gene expression by using the deactivated Cas9-VPR/gRNA system, related to Figure 6. **A**, The diagram of dCas9-VPR complex targeting Vsig4 gene's promoter region with guide RNA-Vsig4. **B**, CRIg abundance in adrenal glands of 16wks HFD WT mice after 4wks treatment with lentivirus carrying dCas9-VPR and gRNA-Vsig4. Data are presented as mean ± SEM. P value is determined by unpaired two-side Student's t-test (B).

References

1. Henry SL, Barzel B, Wood-Bradley RJ, Burke SL, Head GA and Armitage JA. Developmental origins of obesity-related hypertension. *Clin Exp Pharmacol Physiol*. 2012;39:799-806.
2. Kotchen TA. Obesity-related hypertension: epidemiology, pathophysiology, and clinical management. *Am J Hypertens*. 2010;23:1170-8.
3. Troisi RJ, Weiss ST, Parker DR, Sparrow D, Young JB and Landsberg L. Relation of obesity and diet to sympathetic nervous system activity. *Hypertension*. 1991;17:669-77.
4. Sowers JR, Nyby M, Stern N, Beck F, Baron S, Catania R and Vlachis N. Blood pressure and hormone changes associated with weight reduction in the obese. *Hypertension*. 1982;4:686-91.
5. Gudbjornsdottir S, Friberg P, Elam M, Attvall S, Lonnroth P and Wallin BG. The effect of metformin and insulin on sympathetic nerve activity, norepinephrine spillover and blood pressure in obese, insulin resistant, normoglycemic, hypertensive men. *Blood Press*. 1994;3:394-403.
6. Reisin E, Weir MR, Falkner B, Hutchinson HG, Anzalone DA and Tuck ML. Lisinopril versus hydrochlorothiazide in obese hypertensive patients: a multicenter placebo-controlled trial. Treatment in Obese Patients With Hypertension (TROPHY) Study Group. *Hypertension*. 1997;30:140-5.
7. Raitakari M, Ilvonen T, Ahotupa M, Lehtimaki T, Harmoinen A, Suominen P, Elo J, Hartiala J and Raitakari OT. Weight reduction with very-low-caloric diet and endothelial function in overweight adults: role of plasma glucose. *Arterioscler Thromb Vasc Biol*. 2004;24:124-8.
8. Sugerman H, Windsor A, Bessos M and Wolfe L. Intra-abdominal pressure, sagittal abdominal diameter and obesity comorbidity. *J Intern Med*. 1997;241:71-9.
9. Reimann M, Qin N, Gruber M, Bornstein SR, Kirschbaum C, Ziemssen T and Eisenhofer G. Adrenal medullary dysfunction as a feature of obesity. *Int J Obes (Lond)*. 2017;41:714-721.
10. Byrne CJ, Khurana S, Kumar A and Tai TC. Inflammatory Signaling in Hypertension: Regulation of Adrenal Catecholamine Biosynthesis. *Front Endocrinol (Lausanne)*. 2018;9:343.
11. Lee YS, Wollam J and Olefsky JM. An Integrated View of Immunometabolism. *Cell*. 2018;172:22-40.
12. McMaster WG, Kirabo A, Madhur MS and Harrison DG. Inflammation, immunity, and hypertensive end-organ damage. *Circ Res*. 2015;116:1022-33.
13. Levy M, Kolodziejczyk AA, Thaiss CA and Elinav E. Dysbiosis and the immune system. *Nat Rev Immunol*. 2017;17:219-232.
14. Cani PD, Amar J, Iglesias MA, Poggi M, Knauf C, Bastelica D, Neyrinck AM, Fava F, Tuohy KM, Chabo C, Waget A, Delmee E, Cousin B, Sulpice T, Chamontin B, Ferrieres J, Tanti JF, Gibson GR, Casteilla L, Delzenne NM, Alessi MC and Burcelin R. Metabolic endotoxemia initiates obesity and insulin resistance. *Diabetes*. 2007;56:1761-72.
15. Jin X, Yu CH, Lv GC and Li YM. Increased intestinal permeability in pathogenesis and progress of nonalcoholic steatohepatitis in rats. *World J Gastroenterol*. 2007;13:1732-6.
16. Johnson AM, Costanzo A, Gareau MG, Armando AM, Quehenberger O, Jameson JM and Olefsky JM. High fat diet causes depletion of intestinal eosinophils associated with intestinal permeability. *PLoS One*. 2015;10:e0122195.
17. Thaiss CA, Levy M, Grosheva I, Zheng D, Soffer E, Blacher E, Braverman S, Tengeler AC, Barak O, Elazar M, Ben-Zeev R, Lehavi-Regev D, Katz MN, Pevsner-Fischer M, Gertler A, Halpern Z, Harmelin A, Aamar S, Serradas P, Grosfeld A, Shapiro H, Geiger B and Elinav E. Hyperglycemia drives intestinal barrier dysfunction and risk for enteric infection. *Science*. 2018;359:1376-1383.
18. Tilg H, Zmora N, Adolph TE and Elinav E. The intestinal microbiota fuelling metabolic inflammation. *Nat Rev Immunol*. 2020;20:40-54.
19. Puri P, Liangpunsakul S, Christensen JE, Shah VH, Kamath PS, Gores GJ, Walker S, Comerford M, Katz B, Borst A, Yu Q, Kumar DP, Mirshahi F, Radaeva S, Chalasani NP, Crabb DW, Sanyal AJ and Consortium T. The circulating microbiome signature and inferred functional metagenomics in alcoholic hepatitis. *Hepatology*. 2018;67:1284-1302.

20. Lelouvier B, Servant F, Paisse S, Brunet AC, Benyahya S, Serino M, Valle C, Ortiz MR, Puig J, Courtney M, Federici M, Fernandez-Real JM, Burcelin R and Amar J. Changes in blood microbiota profiles associated with liver fibrosis in obese patients: A pilot analysis. *Hepatology*. 2016;64:2015-2027.
21. Amar J, Chabo C, Waget A, Klopp P, Vachoux C, Bermudez-Humaran LG, Smirnova N, Berge M, Sulpice T, Lahtinen S, Ouwehand A, Langella P, Rautonen N, Sansonetti PJ and Burcelin R. Intestinal mucosal adherence and translocation of commensal bacteria at the early onset of type 2 diabetes: molecular mechanisms and probiotic treatment. *EMBO Mol Med*. 2011;3:559-72.
22. Anhê FF, Jensen, B.A.H., Varin, T.V. et al. Type 2 diabetes influences bacterial tissue compartmentalisation in human obesity. *Nat Metab*. 2020;2:233–242.
23. Ortiz S, Zapater P, Estrada JL, Enriquez P, Rey M, Abad A, Such J, Lluis F and Frances R. Bacterial DNA translocation holds increased insulin resistance and systemic inflammatory levels in morbid obese patients. *J Clin Endocrinol Metab*. 2014;99:2575-83.
24. Oh TG, Kim SM, Caussy C, Fu T, Guo J, Bassirian S, Singh S, Madamba EV, Bettencourt R, Richards L, Raffatellu M, Dorrestein PC, Yu RT, Atkins AR, Huan T, Brenner DA, Sirlin CB, Knight R, Downes M, Evans RM and Loomba R. A Universal Gut-Microbiome-Derived Signature Predicts Cirrhosis. *Cell Metab*. 2020.
25. Mathieu M, Martin-Jaular L, Lavieu G and Thery C. Specificities of secretion and uptake of exosomes and other extracellular vesicles for cell-to-cell communication. *Nat Cell Biol*. 2019;21:9-17.
26. Liu Y, Defourny KAY, Smid EJ and Abee T. Gram-Positive Bacterial Extracellular Vesicles and Their Impact on Health and Disease. *Front Microbiol*. 2018;9:1502.
27. Chelakkot C, Choi Y, Kim DK, Park HT, Ghim J, Kwon Y, Jeon J, Kim MS, Jee YK, Gho YS, Park HS, Kim YK and Ryu SH. Akkermansia muciniphila-derived extracellular vesicles influence gut permeability through the regulation of tight junctions. *Exp Mol Med*. 2018;50:e450.
28. Luo Z, Ji Y, Gao H, Gomes Dos Reis FC, Bandyopadhyay G, Jin Z, Ly C, Chang YJ, Zhang D, Kumar D and Ying W. CRIg(+) Macrophages Prevent Gut Microbial DNA-Containing Extracellular Vesicle-Induced Tissue Inflammation and Insulin Resistance. *Gastroenterology*. 2021;160:863-874.
29. Zeng Z, Surewaard BG, Wong CH, Geoghegan JA, Jenne CN and Kubes P. CRIg Functions as a Macrophage Pattern Recognition Receptor to Directly Bind and Capture Blood-Borne Gram-Positive Bacteria. *Cell Host Microbe*. 2016;20:99-106.
30. Helmy KY, Katschke KJ, Jr., Gorgani NN, Kljavin NM, Elliott JM, Diehl L, Scales SJ, Ghilardi N and van Lookeren Campagne M. CRIg: a macrophage complement receptor required for phagocytosis of circulating pathogens. *Cell*. 2006;124:915-27.
31. He JQ, Katschke KJ, Jr., Gribling P, Suto E, Lee WP, Diehl L, Eastham-Anderson J, Ponakala A, Komuves L, Egen JG and van Lookeren Campagne M. CRIg mediates early Kupffer cell responses to adenovirus. *J Leukoc Biol*. 2013;93:301-6.
32. Gorgani NN, He JQ, Katschke KJ, Jr., Helmy KY, Xi H, Steffek M, Hass PE and van Lookeren Campagne M. Complement receptor of the Ig superfamily enhances complement-mediated phagocytosis in a subpopulation of tissue resident macrophages. *J Immunol*. 2008;181:7902-8.
33. Gorgani NN, Thathaisong U, Mukaro VR, Poungpair O, Tirimacco A, Hii CS and Ferrante A. Regulation of CRIg expression and phagocytosis in human macrophages by arachidonate, dexamethasone, and cytokines. *Am J Pathol*. 2011;179:1310-8.
34. Fu W, Wojtkiewicz G, Weissleder R, Benoist C and Mathis D. Early window of diabetes determinism in NOD mice, dependent on the complement receptor CRIg, identified by noninvasive imaging. *Nat Immunol*. 2012;13:361-8.
35. Yuan X, Yang BH, Dong Y, Yamamura A and Fu W. CRIg, a tissue-resident macrophage specific immune checkpoint molecule, promotes immunological tolerance in NOD mice, via a dual role in effector and regulatory T cells. *Elife*. 2017;6.
36. Ying W, Tang K, Avolio E, Schilling JM, Pasqua T, Liu MA, Cheng H, Gao H, Zhang J, Mahata S, Ko MS, Bandyopadhyay G, Das S, Roth DM, Sahoo D, Webster NJG, Sheikh F, Ghosh G, Patel HH,

Ghosh P, van den Bogaart G and Mahata SK. Immunosuppression of Macrophages Underlies the Cardioprotective Effects of CST (Catestatin). *Hypertension*. 2021;77:1670-1682.
37. Kolski-Andreaco A, Cai H, Currle DS, Chandy KG and Chow RH. Mouse adrenal chromaffin cell isolation. *J Vis Exp*. 2007:129.
38. Lukewich MK and Lomax AE. Endotoxemia enhances catecholamine secretion from male mouse adrenal chromaffin cells through an increase in Ca(2+) release from the endoplasmic reticulum. *Endocrinology*. 2014;155:180-92.
39. Ahn J and Barber GN. STING signaling and host defense against microbial infection. *Exp Mol Med*. 2019;51:1-10.
40. Ablasser A and Chen ZJ. cGAS in action: Expanding roles in immunity and inflammation. *Science*. 2019;363.
41. Cheng AW, Wang H, Yang H, Shi L, Katz Y, Theunissen TW, Rangarajan S, Shivalila CS, Dadon DB and Jaenisch R. Multiplexed activation of endogenous genes by CRISPR-on, an RNA-guided transcriptional activator system. *Cell Res*. 2013;23:1163-71.
42. Gilbert LA, Horlbeck MA, Adamson B, Villalta JE, Chen Y, Whitehead EH, Guimaraes C, Panning B, Ploegh HL, Bassik MC, Qi LS, Kampmann M and Weissman JS. Genome-Scale CRISPR-Mediated Control of Gene Repression and Activation. *Cell*. 2014;159:647-61.
43. Konermann S, Brigham MD, Trevino AE, Joung J, Abudayyeh OO, Barcena C, Hsu PD, Habib N, Gootenberg JS, Nishimasu H, Nureki O and Zhang F. Genome-scale transcriptional activation by an engineered CRISPR-Cas9 complex. *Nature*. 2015;517:583-8.
44. Chavez A, Scheiman J, Vora S, Pruitt BW, Tuttle M, E PRI, Lin S, Kiani S, Guzman CD, Wiegand DJ, Ter-Ovanesyan D, Braff JL, Davidsohn N, Housden BE, Perrimon N, Weiss R, Aach J, Collins JJ and Church GM. Highly efficient Cas9-mediated transcriptional programming. *Nat Methods*. 2015;12:326-8.
45. Kotsis V, Stabouli S, Papakatsika S, Rizos Z and Parati G. Mechanisms of obesity-induced hypertension. *Hypertens Res*. 2010;33:386-93.
46. Wirix AJ, Kaspers PJ, Nauta J, Chinapaw MJ and Kist-van Holthe JE. Pathophysiology of hypertension in obese children: a systematic review. *Obes Rev*. 2015;16:831-42.
47. Lambert EA, Straznicky NE, Dixon JB and Lambert GW. Should the sympathetic nervous system be a target to improve cardiometabolic risk in obesity? *Am J Physiol Heart Circ Physiol*. 2015;309:H244-58.
48. Thorp AA and Schlaich MP. Relevance of Sympathetic Nervous System Activation in Obesity and Metabolic Syndrome. *J Diabetes Res*. 2015;2015:341583.
49. Reisin E and Jack AV. Obesity and hypertension: mechanisms, cardio-renal consequences, and therapeutic approaches. *Med Clin North Am*. 2009;93:733-51.
50. Hall JE, do Carmo JM, da Silva AA, Wang Z and Hall ME. Obesity-induced hypertension: interaction of neurohumoral and renal mechanisms. *Circ Res*. 2015;116:991-1006.
51. Schierwagen R, Alvarez-Silva C, Madsen MSA, Kolbe CC, Meyer C, Thomas D, Uschner FE, Magdaleno F, Jansen C, Pohlmann A, Praktiknjo M, Hischebeth GT, Molitor E, Latz E, Lelouvier B, Trebicka J and Arumugam M. Circulating microbiome in blood of different circulatory compartments. *Gut*. 2019;68:578-580.
52. Zulian A, Cancello R, Cesana E, Rizzi E, Consolandi C, Severgnini M, Panizzo V, Di Blasio AM, Micheletto G and Invitti C. Adipose tissue microbiota in humans: an open issue. *Int J Obes (Lond)*. 2016;40:1643-1648.
53. Kimura I, Miyamoto J, Ohue-Kitano R, Watanabe K, Yamada T, Onuki M, Aoki R, Isobe Y, Kashihara D, Inoue D, Inaba A, Takamura Y, Taira S, Kumaki S, Watanabe M, Ito M, Nakagawa F, Irie J, Kakuta H, Shinohara M, Iwatsuki K, Tsujimoto G, Ohno H, Arita M, Itoh H and Hase K. Maternal gut microbiota in pregnancy influences offspring metabolic phenotype in mice. *Science*. 2020;367.
54. Vuong HE, Pronovost GN, Williams DW, Coley EJL, Siegler EL, Qiu A, Kazantsev M, Wilson CJ, Rendon T and Hsiao EY. The maternal microbiome modulates fetal neurodevelopment in mice.

Nature. 2020;586:281-286.
55. Call GB, Husein OF, McIlmoil CJ, Adams A, Heckmann RA and Judd AM. Bovine adrenal cells secrete interleukin-6 and tumor necrosis factor in vitro. *Gen Comp Endocrinol*. 2000;118:249-61.
56. Gonzalez-Hernandez JA, Ehrhart-Bornstein M, Spath-Schwalbe E, Scherbaum WA and Bornstein SR. Human adrenal cells express tumor necrosis factor-alpha messenger ribonucleic acid: evidence for paracrine control of adrenal function. *J Clin Endocrinol Metab*. 1996;81:807-13.
57. Willenberg HS, Path G, Vogeli TA, Scherbaum WA and Bornstein SR. Role of interleukin-6 in stress response in normal and tumorous adrenal cells and during chronic inflammation. *Ann N Y Acad Sci*. 2002;966:304-14.
58. Douglas SA, Sreenivasan D, Carman FH and Bunn SJ. Cytokine interactions with adrenal medullary chromaffin cells. *Cell Mol Neurobiol*. 2010;30:1467-75.
59. Perez-Rodriguez R, Roncero C, Olivan AM, Gonzalez MP and Oset-Gasque MJ. Signaling mechanisms of interferon gamma induced apoptosis in chromaffin cells: involvement of nNOS, iNOS, and NFkappaB. *J Neurochem*. 2009;108:1083-96.
60. Samal B, Ait-Ali D, Bunn S, Mustafa T and Eiden LE. Discrete signal transduction pathway utilization by a neuropeptide (PACAP) and a cytokine (TNF-alpha) first messenger in chromaffin cells, inferred from coupled transcriptome-promoter analysis of regulated gene cohorts. *Peptides*. 2013;45:48-60.
61. Ait-Ali D, Turquier V, Tanguy Y, Thouennon E, Ghzili H, Mounien L, Derambure C, Jegou S, Salier JP, Vaudry H, Eiden LE and Anouar Y. Tumor necrosis factor (TNF)-alpha persistently activates nuclear factor-kappaB signaling through the type 2 TNF receptor in chromaffin cells: implications for long-term regulation of neuropeptide gene expression in inflammation. *Endocrinology*. 2008;149:2840-52.
62. Hemmi H, Takeuchi O, Kawai T, Kaisho T, Sato S, Sanjo H, Matsumoto M, Hoshino K, Wagner H, Takeda K and Akira S. A Toll-like receptor recognizes bacterial DNA. *Nature*. 2000;408:740-5.
63. Hornung V, Ablasser A, Charrel-Dennis M, Bauernfeind F, Horvath G, Caffrey DR, Latz E and Fitzgerald KA. AIM2 recognizes cytosolic dsDNA and forms a caspase-1-activating inflammasome with ASC. *Nature*. 2009;458:514-8.
64. Hoelzer K, Shackelton LA and Parrish CR. Presence and role of cytosine methylation in DNA viruses of animals. *Nucleic Acids Res*. 2008;36:2825-37.